Post-synthesis modifications of two-dimensional MoSe2 or MoTe2 by incorporation of excess metal atoms into the crystal structure

Coelho, P. M.; Komsa, H.-P.; Diaz, H. C.; Ma, Y.; Krasheninnikov, A. V.; Batzill, M.;

Originally published:

April 2018

ACS Nano 12(2018), 3975-3984

DOI: https://doi.org/10.1021/acsnano.8b01580

Post-synthesis modifications of two-dimensional $MoSe_2$ or $MoTe_2$ by incorporation of excess metal atoms into the crystal structure

Paula Mariel Coelho,[1] Hannu-Pekka Komsa,[2] Horacio Coy Diaz,[1] Yujing Ma,[1] Arkady V. Krasheninnikov,[3,2] Matthias Batzill[1,#]

[1] Department of Physics, University of South Florida, Tampa, FL 33620, USA.

[2] Department of Applied Physics, Aalto University, 00076 Aalto, Finland.

[3] Institute of Ion Beam Physics and Materials Research, Helmholtz-Zentrum Dresden-Rossendorf, 01328 Dresden, Germany.

Phase engineering has extensively been used to achieve metallization of 2D semiconducting materials, as it should boost their catalytic properties or improve electrical contacts. Such structural phase changes may however be difficult to control and maintain under changing conditions. In contrast, here we demonstrate compositional phase change by incorporation of excess metals into the crystal structure. We demonstrate post-synthesis restructuring of the semiconducting $MoTe_2$ or $MoSe_2$ host-material by unexpected easy incorporation of excess Mo into their crystal planes, which causes local metallization. The amount of excess Mo can reach values as high as 10% in $MoTe_2$ justifying its categorization as a novel metallic 2D material. The incorporation mechanism is explained by density functional theory in terms of the energy difference of Mo atoms incorporated in the line-phases as compared to Mo ad-clusters. Angle resolved photoemission spectroscopy reveals that the incorporated excess Mo induces band gap states up to the Fermi-level causing its pinning at these electronic states. The incorporation of excess transition metals in $MoTe_2$ and $MoSe_2$ is not limited to molybdenum, but other transition metals can also diffuse into the lattice, as demonstrated experimentally by Ti deposition. The mechanism of incorporation of transition metals in $MoSe_2$ and $MoTe_2$ is revealed, which should help to address the challenges in synthesizing defect free single layer materials by, for example, molecular beam epitaxy. The easy incorporation of metal atoms into the crystal also indicates that the previously assumed picture of a sharp metal/2D-material interface may not be correct, and at least for $MoSe_2$ and $MoTe_2$ in-diffusion of metals from metal-contacts into the 2D material has to be considered. Most importantly though, the process of incorporation of transition metals with high concentrations into pristine 2D transition metal dichalcogenides enables a new pathway for their post-synthesis modifications and adding new functionalities.

Keywords: Transition Metal Dichalcogenides; Crystal Modifications; Metal Contacts; Inversion Domains; Grain Boundaries; Metal Interstitials.

[#]: corresponding author e-mail: mbatzill@usf.edu

Atomic structure engineering of two dimensional (2D) materials by introducing dopants,[1,2] point-defects,[3] inducing phase transitions,[4,5,6,7] alloying,[8] creating in-plane interfaces[9,10] or boundaries between grains[11,12,13,14,15,16,17] enables addition of new functionalities to these materials. As for the latter, mirror twin boundaries (MTBs) between grains rotated by 60° have been found in Mo-based transition metal dichalcogenides (TMDs), and identified as new Mo-rich one dimensional (1D) structures.[11,12,11,16,18] These structural modifications can be prominent in monolayers of $MoSe_2$ and $MoTe_2$ grown by molecular beam epitaxy.[19, 20] Interestingly, it has been shown by density-functional theory (DFT) calculations [11,21] and experimentally observed[22,23] that MTBs exhibit metallic electronic bands with finite dispersion. Because of the confinement of the metallic states, they show intriguing 1D quantum liquid behavior described by the Tomonaga-Luttinger liquid theory and are the first 1D metal for which spin-charge separation has been experimentally confirmed.[22] Also, as expected for 1D metals, a Peierls' metal-to-insulator instability has been observed with transition temperature of ~230 K for $MoSe_2$.[22,23]

2D-materials consist of surface only and consequently their stoichiometry and morphology can be modified more easily as compared to bulk systems[24] and this potentially enables tuning of their properties over a wider range, adding to the functionalities of 2D materials. Post-synthesis phase change of MoS_2 or $MoTe_2$ from the semiconducting 2H to metallic 1T or 1T' structures by charge doping or thermal processing has been suggested to modify their catalytic properties[25,26] as well as an approach for making better electrical contacts to 2D materials. [6,27,28,29] Long term phase stability and/or stability at the interfaces as well as processing conditions are, however, potential limitations of such phase engineering methods. Thus, crystal engineering by the introduction of dense MTB networks by locally controlled post-synthesis stoichiometry modifications could be an alternative approach for the introduction of metal contacts in 2D materials and to tune chemical functionalities. So far, the mechanism of formation of MTB networks is not understood and consequently no process of their controlled formation has been demonstrated. Here we show that incorporation of excess Mo into $MoSe_2$ or $MoTe_2$ lattice, but not MoS_2, results in the self-formation of MTB networks. We also demonstrate that the incorporation of excess metals into $MoTe_2$ is not limited to Mo: other transition metals, namely Ti, are also readily incorporated in this 2D material at interstitial sites.

Results and Discussion

In previous studies of mono- to few- layer $MoSe_2$ or $MoTe_2$ growth by molecular beam epitaxy (MBE) the formation of MTB networks were observed by various groups.[11,16,19,22,23,30] Although the structure and composition of these MTBs were determined by transmission electron microscopy, the origin and

mechanism for their formation remained unresolved. Contrary to other types of grain boundaries that require rotation of neighboring grains, MTBs can be viewed as 1D compositional modifications of the TMD lattice. The relationship between the atomic structure of a pristine TMD sheet and that with an inversion domain (ID) and the associated MTB is shown in Fig. 1(a). Schematically, extra Mo atoms form a line, then a part of the Mo sub-lattice is translated relative to the rest of the system, thus creating an ID without the need of a lattice rotation. This simple model suggests that MTB triangular loops and eventually dense networks of MTBS may be formed by incorporation of excess Mo into the crystal structure. This begs the question if the observed MTB networks in MBE grown samples are formed during growth, for instance by coalescence of twin grains, or if such networks can form 'post-growth' by incorporation of excess Mo (note that elemental Mo is constantly supplied during MBE- growth) into the already grown $MoSe_2$ or $MoTe_2$ film. Here we demonstrate that the latter is the case by facilitating MTB formation by deposition of Mo onto a pristine single crystal surface, i.e. without any growth process of $MoSe_2$ or $MoTe_2$. This astonishing result is confirmed by DFT calculations and has several important implications, specifically it allows for controlled post-synthesis crystal modifications.

Formation of MTB networks by incorporation of excess Mo into the lattice. To address the question if layered materials can be modified with MTB networks by incorporation of excess Mo, we start with single crystals of MoS_2, $MoSe_2$, or $MoTe_2$ and deposit elemental Mo from a high purity Mo-rod with an e-beam evaporator under ultrahigh vacuum. Before deposition the surfaces show only isolated defects that are well-documented in the literature to occur on single crystals.[31] Atomic resolution STM images reveal well-ordered crystalline surfaces as shown in Fig. 2. The figure also presents STM images for sequential deposition of Mo on these three different Mo-dichalcogenide single crystal surfaces at 350°C. With increasing Mo-deposition the three surfaces evolve differently. On both $MoTe_2$ and $MoSe_2$ triangular MTB-loops form, while on MoS_2 only formation of metal clusters is observed. In high resolution filled state images the triangular defects in $MoSe_2$ and $MoTe_2$ appear as two bright parallel lines. The STM images of such structures are illustrated by the example of $MoSe_2$ in Fig. 1(b). To demonstrate that these two parallel lines correspond to MTBs we performed Tersoff-Hamann simulations of the STM images of an ID separated by MTBs shown in Fig. 1(c). These simulations reveal the same double row structure indicating that in filled state images the chalcogen atoms adjacent to the actual MTBs are imaged 'bright'. The excellent match between the experimental STM data and the simulated ones for MTBs confirms that the line-structures formed by Mo depositions in $MoSe_2$ and $MoTe_2$ are indeed MTB loops. This is also consistent with previously reported STM images of MTBs in MBE grown monolayers.[19,20,22,23] In our experiment, deposition of Mo on $MoSe_2$ eventually results in the formation of Mo ad-clusters. The

transition from formation of triangular MTB loops to nucleation of Mo-clusters occurs at ~0.05 ML of excess Mo for the growth conditions in this experiment. The Mo-clusters preferentially nucleate at the corners of the triangular MTB-loops, indicating that these are high energy sites for metal nucleation. On $MoTe_2$, on the other hand, the density of the MTB network keeps increasing beyond the saturation coverage observed for $MoSe_2$. We observe that 15-20% of a ML of excess Mo can be incorporated into $MoTe_2$. Further deposition eventually also results in the formation of Mo-clusters at the surface. The higher Mo-concentration in the MTBs implies that for $MoTe_2$ and for $MoSe_2$, but not for MoS_2, Mo atoms can readily diffuse into the crystal plane of the TMD and self-organize into ordered 1D crystal structures embedded in the TMD lattice.

MTBs can also be obtained by RT deposition of Mo and subsequent annealing. Deposition of a small amount of Mo (1 excess-Mo/ 200 unit cells) at RT forms point like defects in $MoTe_2$ as shown in Fig. 3(a). The inset in Fig. 3a shows high-resolution images that indicate that these point defects appear as three short bright lines in filled state images. Only one kind of defect configuration are observed after RT deposition. The contrast observed in STM suggests that these are single Mo-interstitial sites. Like demonstrated above for the MTBs, it is the chalcogen atoms adjacent to the defect site that appears bright in STM. Fig. 4 shows a detailed STM image of a single protrusion. It appears that the center is imaged dark if filled states are probed. This dark center is surrounded by three bright protrusions that form almost a complete triangle. Key features of this experimental image are reproduced by Tersoff-Hamann STM simulations of a Mo-interstitial as shown in Fig. 4 (c) and (d). The simulations also show a dark center surrounded by 3 bright spots. In the inset of Fig. 3a, it is also apparent that atoms surrounding the interstitial site appears slightly brighter. This region of brighter contrast in filled state images extends to ~2 nm away from the interstitial sites. This change in contrast is most likely associated with a local band bending induced by a charged defect site. Bright contrast in filled state STM images suggest a local upward band bending and thus negatively charged interstitial site in $MoTe_2$. Importantly, while after room temperature deposition, almost exclusively individual interstitial sites are detected, these interstitials appear to agglomerate into triangular MTB loops, as shown in Fig. 3(b), after annealing of the sample to 250 °C. From the initial density of bright protrusions in the STM image after room temperature deposition and the length of line defects after annealing it is apparent that each initial protrusion converts into ~ 1nm of MTB loop length. This conversion is consistent with the schematic in Fig. 1, provided that every initial protrusion corresponded to one excess Mo-atom. This further verifies our assignment of the protrusions to a single Mo-interstitial. Importantly, the formation of MTBs by annealing to 250 °C suggests sufficient mobility of the Mo interstitials to aggregate into MTBs.

The experiments demonstrate that excess Mo modifies the lattice structure of $MoSe_2$ and $MoTe_2$ with metallic 1D-structural motifs. For MoS_2 this process does not occur. To gain insight on the energetics of this process and potential pathways for the formation of extended MTBs we performed detailed DFT simulations.

Comparison of formation energies of excess Mo in ad- or interstitial-sites. First, we compare the formation energies of Mo-adatoms with those of two kinds of Mo-interstitials in the Mo-dichalcogenide lattice, as shown in Fig. 5 (a). Formation energy for the system containing n_{Mo} additional Mo atoms is defined as $E_f = E(\mathrm{defect}) - E(\mathrm{pristine}) - n_{\mathrm{Mo}}\mu_{\mathrm{Mo}}$, where $E(\mathrm{defect})$ is the total energy of the system with extra Mo atoms, $E(\mathrm{pristine})$ is the energy of the pristine system, and Mo chemical potential μ_{Mo} is chosen depending on the deposition stage. We considered a split interstitial site, i.e. the occupation of the regular Mo-site with two Mo-atoms and a regular interstitial site in the center of the hexagonal structure. For all Mo-dichalcogenides formation of interstitials or split interstitials is favored over ad-atoms, as evident from Table 1. $MoTe_2$ prefers the regular interstitial site, while $MoSe_2$ and MoS_2 prefer split interstitial sites. Thus, single Mo atoms should always have a tendency to be incorporated into the lattice. Only a modest potential kinetic barrier has to be overcome for the excess Mo to go from an ad-atom site to an interstitial site, which we have estimated to be 0.6, 0.2, and 0.4 eV for MoS_2, $MoSe_2$, and $MoTe_2$, respectively (see supplementary information). With increasing Mo deposition, the formation energy of interstitials or pairs of interstitials should, however, be compared to the formation energy of adsorbed dimers or Mo-clusters rather than individual ad-atoms. The energy difference determines if the interstitials are still energetically favored over adsorbed Mo-clusters, i.e. if it remains energetically favorable for two (split) interstitials to remain in the lattice or adsorbed dimers become favored. Comparison of the formation energies, shown in table 1, reveals that only for $MoSe_2$ and $MoTe_2$ the interstitial site is favored over adsorbed Mo- dimers, while for MoS_2 adsorbed Mo-dimers are preferable. Consequently, one would expect that two Mo split-interstitials combine to an adsorbed Mo-dimer for MoS_2. Incorporation of 3 or more excess Mo-atoms allows the formation of MTBs, as indicated in Fig. 5 (d,e).

Formation of MTBs by agglomeration of Mo interstitials: With increasing the number of excess Mo-atoms, or correspondingly the lengths of the MTB loop, the formation energy of the MTB defined as a difference between the total energy of the system with the MTB and pristine system with Mo dimers on its surface decreases for all TMDs, (Fig. 5c), indicating that the formation of MTBs is energetically favorable over dimer formation. As further Mo is deposited on the surface, the proper energy reference for the

MTBs could correspond to larger Mo clusters. However, since this leads to exponentially increasing computational complexity and the structures are likely non-unique, we only consider the limiting case of bulk Mo. In this case, formation energies are positive, but the energy difference for $MoTe_2$ is much lower than for other TMDs, and it is going down with the size of IDs. As the chemical potential of Mo atoms in clusters should be between those in the dimer and bulk crystal, one can expect that IDs and MTBs should easily appear in $MoTe_2$ and hardly in MoS_2, while $MoSe_2$ is an intermediate case, as observed in the experiments.

The decrease in MTB formation energy with increasing ID size implies that it is energetically favorable for an ID to grow in size by incorporating excess Mo atoms. In our experiments we utilize a very low Mo deposition rate that effectively adds one Mo-atom at a time and this facilitates the MTB growth. The observed higher density of MTBs and thus smaller IDs in $MoTe_2$ as compared to $MoSe_2$ may be associated with the lower formation energies in $MoTe_2$, which causes higher nucleation rates. Besides, in $MoSe_2$ it is easier for an isolated Mo split interstitial to 'resurface' and attach to a growing MTB through surface diffusion than in $MoTe_2$. This may also contribute to the larger MTB-loops in $MoSe_2$, like e.g. the one in Fig. 1(b), which contains ~ 50 excess Mo atoms. In $MoSe_2$ the growth of the MTB-loops seems only limited when the growing MTB meets neighboring MTBs, at which point Mo-cluster formation sets in, because the MTB cannot grow any further.

For the growth of MTBs to happen, the energy barriers for adding new Mo-atoms to an existing MTB must be low. Thus, to understand the process of MTB growth, we evaluated kinetic barriers for the diffusion of interstitials and the conversion of interstitials into MTBs. Experimentally we demonstrated that annealing to ~ 500 K is sufficient for the formation of MTBs, suggesting modest barrier for diffusion of Mo-interstitials and the formation of MTB loops. Pathways and barriers for diffusion of interstitials and (split) interstitials in $MoTe_2$ and $MoSe_2$ are illustrated in Fig. S1 and S2, respectively. From these barriers we estimated that Mo interstitials are very mobile in $MoTe_2$ and can diffuse at 200 K, while in $MoSe_2$ split interstitials encounter significantly larger barriers but can diffuse at 600 K. A proposed atomic mechanism for the formation of MTBs by sequential incorporation of excess Mo into the $MoTe_2$ lattice and their energy gains are illustrated in Fig. 6. By adding a Mo atom near the corner of the ID and shifting the neighboring Mo atoms of the MTB to the adjacent interstitial site, the MTB effectively moves by one lattice constant. Fig. 6(d) also shows the energy landscape for the growth from ID size 4 to size 5. The energy decreases with the highest barrier between local energy minima being only about 0.5 eV, thus demonstrating that such process can readily occur. The initial structure is justified by noting that the

energy for adding Mo interstitial near the corner of the MTB loop is favored by 0.25 eV over interstitial being far from it.

Fermi-level pinning by MTB network. The easy incorporation of excess Mo into the lattice of $MoSe_2$ or $MoTe_2$ implies the formation of new electronic states due to the excess Mo-induced MTB networks. It has been previously shown for MTBs in $MoSe_2$ that they exhibit metallic properties and undergo a Peierls transition as expected for 1D metals. A high density of states in the band gap of the semiconducting $MoSe_2$ or $MoTe_2$ implies a pinning of the Fermi-level at these gap-states, not different from the Fermi-level pinning observed at reconstructed semiconductor surfaces or at metal-induced gap states in metal/semiconductor interfaces. Knowledge of the Fermi-level position in MTB modified $MoSe_2$ or $MoTe_2$ thus is crucial if these modifications are going to be used to fabricate controlled metal contacts with defined Fermi-level position. To gain insight in the electronic structure and Fermi-level position of the surface modified by MTBs, we performed ARPES studies. Fig. 7 shows band dispersion along the Γ-K direction of the BZ for single crystal $MoSe_2$ and $MoTe_2$. Note that for single crystals the valence band maximum is at the Γ-point. Both single crystals are n-doped, which is the natural doping of Mo-dichalcogenides and is likely originating from intrinsic defects. After formation of MTBs by deposition of Mo at 350 °C the valence band maximum (VBM) at the Γ-point is shifting closer to the Fermi-level, i.e. it becomes slightly less n-doped. This shift is due to the pinning of the Fermi-level at MTB-induced states. These states are better seen in energy distribution curves (EDCs) measured at the Γ-point and shown in Fig. 7 (c) and (f) for $MoTe_2$ and $MoSe_2$, respectively. The EDCs clearly indicate the band gap states extending up to the Fermi-level and shift of the VBM of 130 meV and 40 meV for $MoTe_2$ and $MoSe_2$, respectively. This means that the VBM at the Γ-point occur at 0.75 eV and 1.0 eV for $MoTe_2$ and $MoSe_2$ for surfaces modified with MTBs. These latter values for the VBM is expected to be independent of the initial doping of the sample since the Fermi-level position in the MTB modified material is pinned at the defect states.

It is worthwhile pointing out that surface modifications with MTBs naturally induces IDs. Such IDs will have different stacking relative to the second layer than the natural 2H-stacking of Mo-dichalcogenides.[32] It is known that the stacking and interlayer interactions does influence the band maximum at the Γ-point. Consequently, there may be a small error in the above measurements at the Γ-point due to broadening of the VBM by the formation of IDs. Thus we performed also measurements for the shift of the VBM at the K-point. The results of these measurements are shown in Fig. S4. The same trend for the shift of the VBM is observed at the K-point as for the Γ-point. However, a slightly larger upward shift of the VBM at the K-

point are measured of 160 meV and 50 meV for $MoTe_2$ and $MoSe_2$, respectively. This slight variation is consistent with a small relative shift of the VBM at the Γ- and K- points due to modifications of interlayer interactions as the consequence of the formation of IDs.

Titanium incorporation into $MoSe_2$ and $MoTe_2$ lattices. The above discussion of the controlled formation of MTBs by Mo deposition shows that this is an approach to locally metallize these materials with defined Fermi-level position with respect to the VBM of the semiconductor parent material. The apparently easy incorporation of Mo into the lattices of $MoSe_2$ and $MoTe_2$ also raises the question if other transition metals may also diffuse into the 2D lattice rather than remaining at the surface. If this was the case, then for example deposition of metal contacts onto TMDs may be inadvertently already modified by transition metals in interstitial sites or by MTB networks underneath of the metal contact patches. This would be a very different scenario to the general simplified view of sharp metal/2D-material interfaces with chemical interactions of the metal with only the topmost chalcogen atoms of the TMD.[33] To address this important issue for metal/TMD interfaces, we study titanium deposition in the ultra-low coverage limit with the goal to investigate if Ti remains at the surface or occupies interstitial sites. Ti and its alloys are prototypical materials used for making well-adhering metal contacts on 2D materials and thus its diffusion into the 2D material would suggest a drastic change in the metal/2D-material interface compared to previous models.

Figure 8 shows the surface of $MoTe_2$ after deposition of ~0.3 % of a ML of Ti with the sample at 350 °C (where 1 ML is defined as the number of Mo-atoms in the $MoTe_2$ monolayer, i.e. 1ML corresponds to one Ti atom per $MoTe_2$ unit cell). We observe mostly small protrusions and only a few triangular MTB-loops. Occasionally, we observe large MTB loops with several of them being aligned, as shown in Fig. 8 (b). Zooming in on the small protrusions, presented in Fig. 8 (c) we identify the same 'ring' structure that we associated with single interstitial atoms for Mo-deposition. This suggests that the protrusions are also due to transition metal interstitials, but in this case they are the consequence of Ti atoms at the interstitial sites in $MoTe_2$ and thus different transition metal interstitials appear to give similar contrast in STM images. It is interesting to point out that for Mo deposition we observe many more MTB loops for the same deposition temperature and similar coverage than for Ti deposition. This implies that Ti-interstitials are less mobile than Mo-interstitials or prefer to stay as single interstitials rather than to agglomerate. The observation of multiple large triangular MTB loops along a line may suggest that these form along preexisting defects in the crystal along which the diffusion may be enhanced. Preferred formation of Ti interstitials compared to Ti- adatoms or Ti in split-interstitial sites is also confirmed by DFT simulations. Our calculations indicate that the formation energy for Ti-interstitials is -4.93 eV and is energetically

favored by 2.59 eV compared to a Ti ad-atom. It is also interesting to note that formation energy for Ti-interstitials is favored as compared to Mo-interstitials (-3.85 eV; see table 1), further stressing the strong preference for Ti to form interstitials in $MoTe_2$. This large formation energy of Ti in the interstitial site may also contribute to its stability and larger barriers for diffusion. In addition, diffusion should proceed via a site exchange of the Ti-interstitial with a Mo lattice atom. We calculate that the configuration of such a site exchange is energetically disfavored by 0.2 eV. While this is a relative small energy, it will add to the barrier of diffusion for Ti.

Finally, ARPES measurements of Ti-modified $MoTe_2$ are shown in Fig. 9. Similar to the case of excess Mo, band gap states are observed that pin the Fermi-level, as can be seen from the EDC at the Γ-point shown in Fig. 9(c). The VBM is measured to be at 0.71 eV below the Fermi-level at the Γ-point for the Ti-modified surface. This is slightly closer to the Fermi-level than for Mo-modified $MoTe_2$ where the VBM was found at 0.75 eV. This indicates that the Fermi-level pinning occurs at slightly different energy in the band gap for Ti-modified $MoTe_2$ than for $MoTe_2$ modified by excess Mo. This shows that for some TMDs the incorporation of excess transition metals into the lattice has to be taken into account when modeling the metal/TMD interface. We stress that the intermixing of the metal with the TMD is not universal. For $MoTe_2$ and $MoSe_2$, it appears that it is their larger unit cell compared to MoS_2 that facilitates the incorporation of excess transition metals in interstitial sites and their subsequent restructuring into one dimensional crystal modifications.

Conclusions

In conclusion, we have shown that the morphology of $MoTe_2$ and to a lesser extent $MoSe_2$ can be altered by incorporation of excess Mo. The excess Mo organizes itself into metallic 1D structures and their dense networks represents novel Mo-rich 2D phases of these materials. The easy incorporation of excess Mo in these materials explains the mechanism responsible for the formation of such MTB networks in MBE grown monolayers of $MoSe_2$ and $MoTe_2$. [16,19,20] Our observations also imply that some of the simple models of metal/TMD interfaces that suggest that the ad-metal only interacts with the topmost chalcogen atoms may need to be reconsidered for certain metal/TMD interfaces. Specifically, our studies show that at least for Ti or Mo interfaces with $MoTe_2$ or $MoSe_2$ the system can be far more complex and metal in-diffusion and crystal modifications may occur. Finally, we want to point out that the understanding of excess metal induced crystal modifications opens new opportunities for further functionalization of TMDs, which may be particularly important for chemical transformation reactions over TMD catalysts.

Methods

Sample preparation: Commercial TMD single crystals (Graphene HQ) were cleaved in air by scotch tape and immediately introduced into the vacuum chamber. The TMDs were outgassed for 2 h at 250 °C. Atomic Mo or Ti was deposited by sublimation of Mo or Ti from a 2mm high purity metal rod. The rod was heated in a water cooled mini e-beam evaporator. We choose a very low Mo-flux that gave a deposition rate of ~ 5 x 10^{-4} ML per minute, where we define one monolayer (ML) as the number of Mo-atoms in a single layer of $MoTe_2$. For Ti deposition a flux of ~2x 10^{-4} ML per minute was measured. This low deposition rates allows for single Mo or Ti atoms to equilibrate with the surface before meeting other deposited metals at the surface. Deposition was carried out with the sample at room temperature or at elevated temperature of 350 °C.

STM characterization: After deposition, the samples were transferred in-situ from the preparation chamber into an analysis chamber for characterization by room temperature scanning tunneling microscopy (STM). The analysis chamber hosts an Omicron STM-1. Electrochemically etched W-tips are used for imaging. The MTB defects are more easily imaged under filled state conditions and the detailed imaging conditions are reported in the STM figures. The contrast of the line-defects is compared to simulated STM images to confirm the structure of the line defects.

ARPES measurements: The analysis chamber also houses a hemispherical analyzer (Scienta R3000) with a 2D detector for angle-resolved photoemission spectroscopy (ARPES) measurements. A re-focused helium discharge lamp providing non-polarized He-I or He-II light is used for the excitation source. All spectra were acquired with the sample at room temperature.

Density functional theory: Density functional theory (DFT) calculations were carried out in the framework of projector-augmented waves as implemented in the VASP code[34]. We adopt PBE exchange-correlation functional and account for spin-polarization throughout. The defective systems are modeled using 10x10 supercells, with the Brillouin zone sampled using solely the Γ-point. Migration barriers are evaluated with the help of climbing-image nudged elastic band approach[35].

Associated Content:

Supplementary materials:

ARPES of pristine and MTB modified $MoTe_2$ and $MoSe_2$; DFT estimation of diffusion barriers.

Author information:

Corresponding author: *e-mail: mbatzill@usf.edu*

Author contribution: *P.M.C., H.C.D., and Y.M. performed the STM and ARPES studies of MTB modified TMDs, H.-P. K. and A.V.K. performed DFT simulations, A.V.K and M.B. directed the research and wrote the paper.*

Notes: *The author declare no competing financial interest.*

Acknowledgements:

The authors acknowledge support from the National Science Foundation under award ECCS-1608654. We thank the Academy of Finland for the support under Projects No. 286279 and 311058. We also thank CSC-IT Center for Science Ltd. and generous grants of computer time and PRACE for awarding us access to Hazel Hen at High Performance Computing Center, University of Stuttgart, Germany.

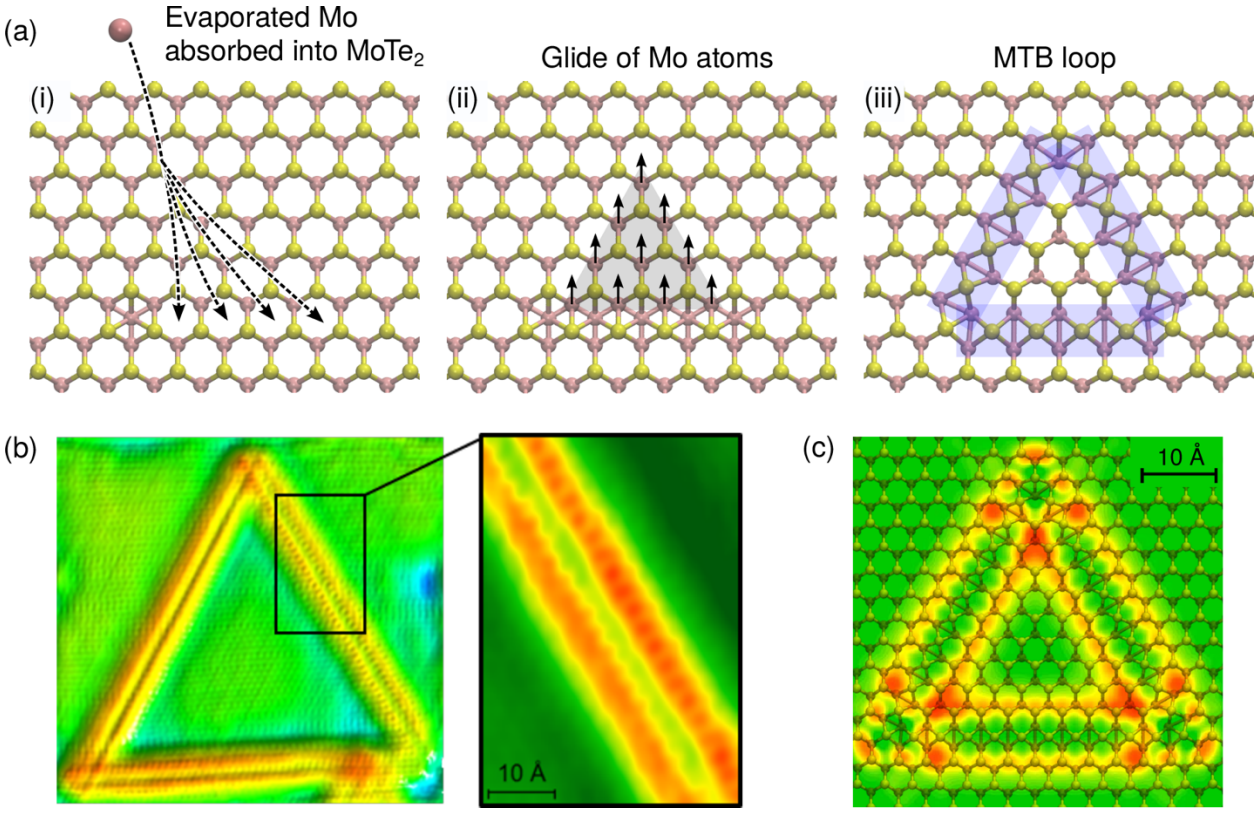

Figure 1. Schematic illustration of the formation of an ID surrounded by an MTB loop by incorporation of excess Mo into the Mo-chalcogenide lattice and its experimental verification in STM. A schematic model for the formation of an ID is shown in (a). Mo-incorporation into the pristine lattice (i) and subsequent translation of a portion of the Mo-sublattice (ii) causes the formation of an ID surrounded by a MTB-loop (iii). Such MTB loops can be observed by STM shown in (b) (V_{bias}:-1.1V; I_t: 0.7nA) for a MTB-loop structure with about 50 added Mo-atoms in $MoSe_2$. The experimental STM image of the double-row structure is reproduced well in Tersoff-Hamann simulated STM images shown in (c). Note that the simulated system is much smaller than the experimental one in panel (b).

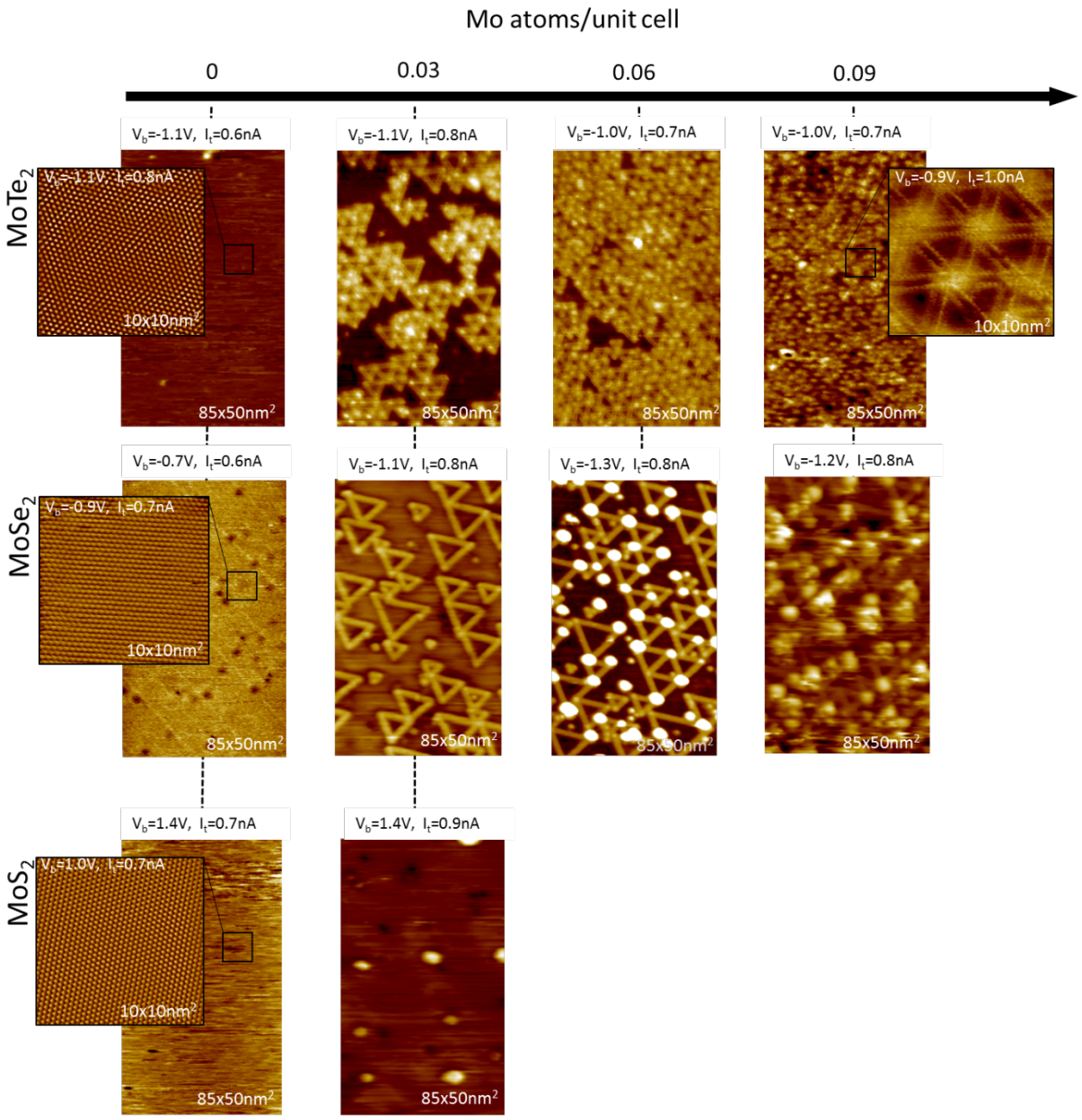

Figure 2. STM images for sequential deposition of Mo at 350˚C on the three different Mo-dichalcogenides substrates. The axis is based on the normalized number of Mo atoms absorbed within the unit cell of $MoTe_2$.

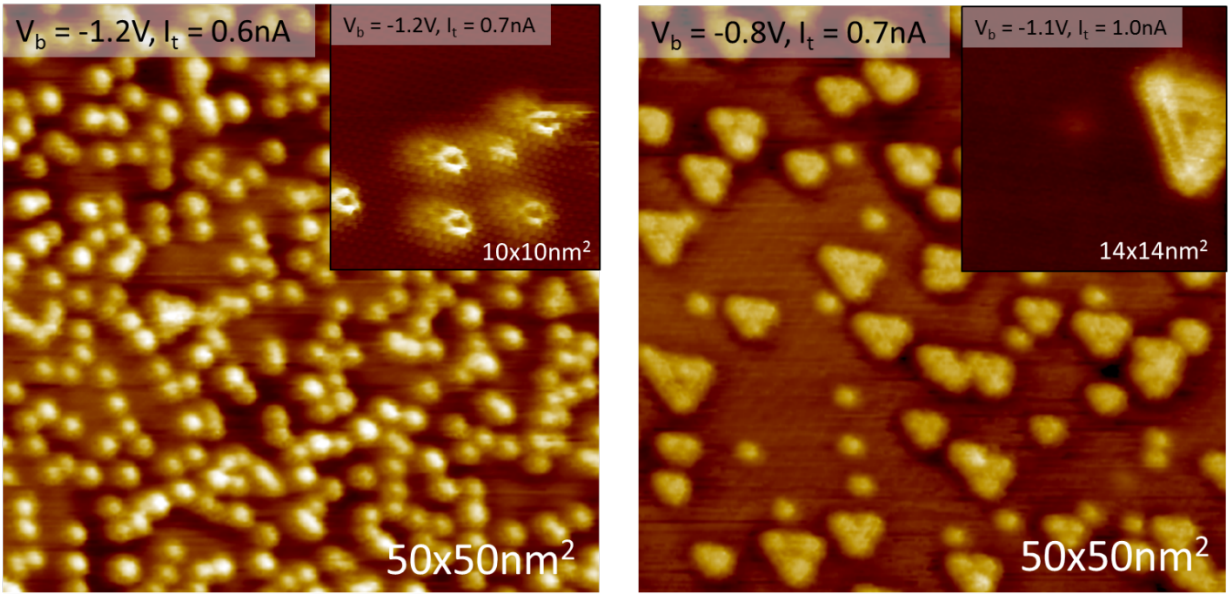

Figure 3. STM studies of $MoTe_2$ surfaces with Mo deposited at room temperature and subsequent annealing. (a) Large scale STM images of $MoTe_2$ after Mo deposition at room temperature. The inset shows the structure of individual Mo-induced point defects (likely Mo-interstitials). (b) Large scale STM images of $MoTe_2$ after annealing at 250˚C. Annealing at such temperature converts the point defect into MTB-loops clearly resolved in the inset.

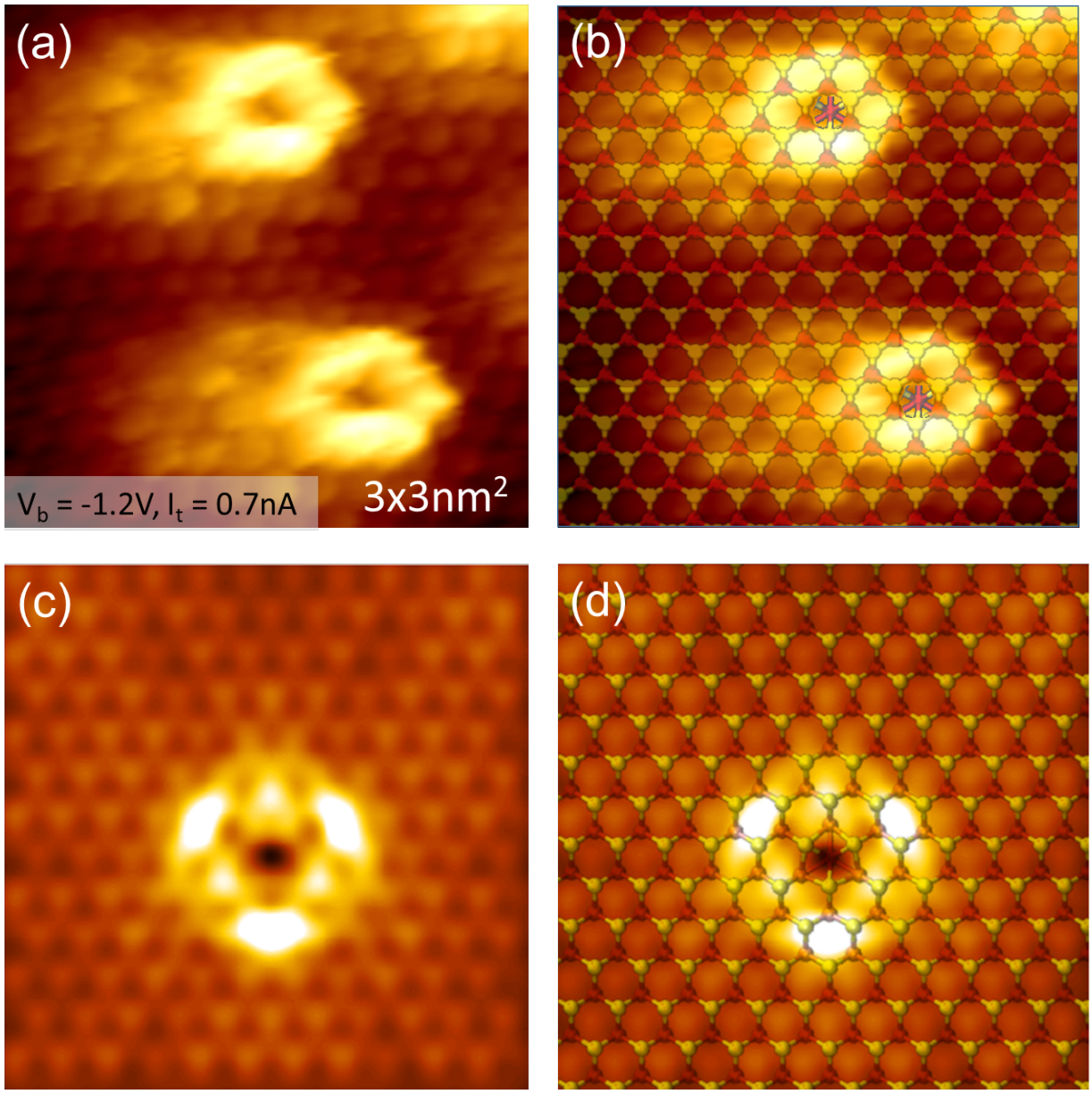

Figure 4: STM of single Mo-interstitial in $MoTe_2$. A filled-state STM image (V_{bias} = -1.2 V) is shown in (a) with a ball-and-stick model overlayed in (b). The dark center of the defect is close to the interstitial site using the atomic corrugation of the surrounding structure as indicators for the Te sub-lattice. Simulated STM images are shown in (c) and in (d) with the superimposed lattice. The important point is that the actual interstitial site is imaged as a depression and the surrounding is imaged brighter in a triangular configuration, in agreement with the experiment.

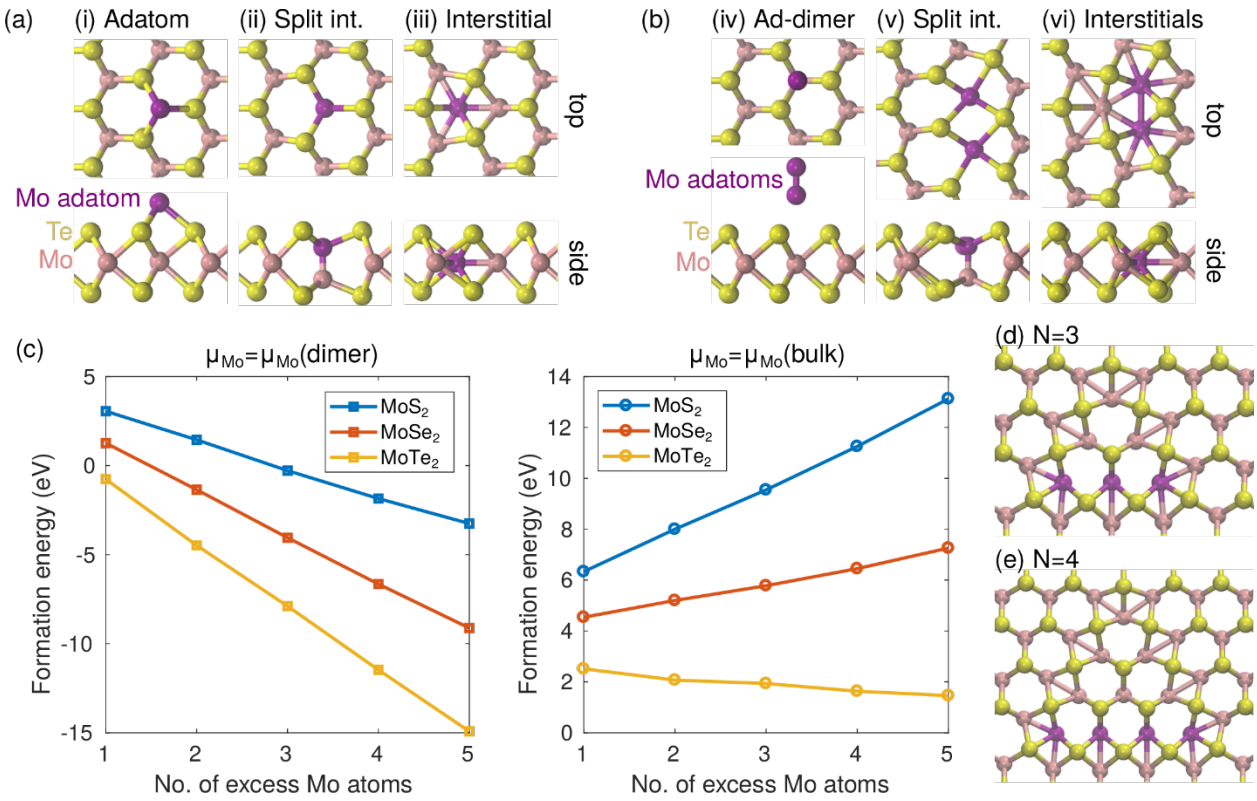

Figure 5. Configurations and formation energies of excess Mo incorporated into Mo-dichalcogenides. (a) Atomic configurations for defects involving a single additional Mo atom in 2D TMDs: (i) adatom, (ii) interstitial, and (iii) split interstitial. (b) Atomic configurations for defects involving two additional Mo atoms: (iv) ad-dimer, (v) a pair of split interstitials in nearest neighbor (NN) sites, and (vi) a pair of NN interstitials. (c) Energy difference between the system with inversion domain and the pristine TMD sheet with a corresponding number of Mo atoms either in the dimer or bulk crystal. (d,e) Atomic structures of inversion domains with 3 and 4 extra Mo atoms.

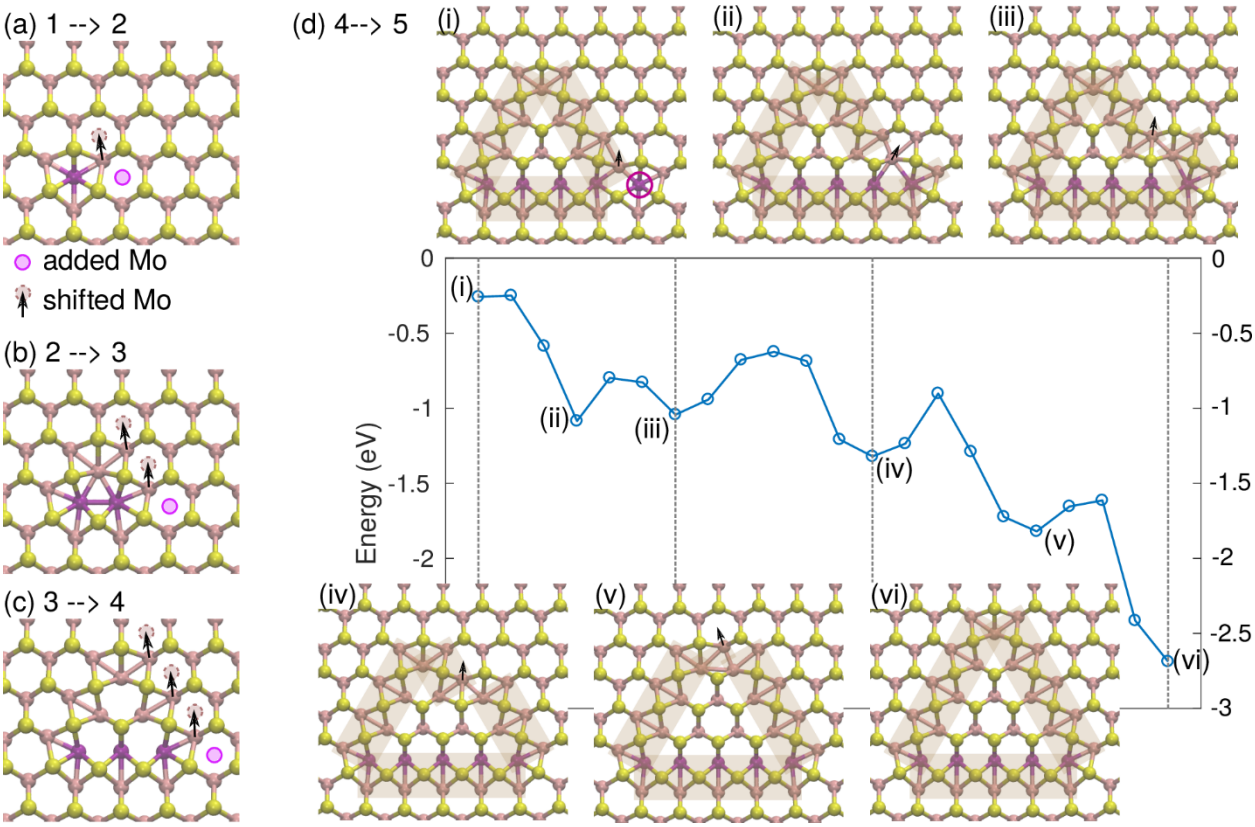

Figure 6. Illustration and energy barriers for the growth of a MTB-loop by addition of an extra excess Mo atom. (a-d) Illustration of the atomic mechanism for the enlargement of the MTB loop (from size N to N+1) by addition of excess Mo (magenta atoms). The magenta circle denotes the position of the next added Mo and the black arrow the subsequent shift of the neighboring Mo atom(s) with the final position shown by brown circles. (d) Atomic configurations and the corresponding energy landscape for the transformation from N=4 to N=5, showing overall decrease in energy. All barriers between local energy minima are within 0.2 - 0.5 eV. Zero energy corresponds to MTB loop of size N=4 and isolated Mo interstitial, indicating that the corner site is more favorable.

	a (Å)	Formation energies (eV) for single excess Mo atom (Fig. 5 (a)) $\mu_{Mo}=\mu_{Mo}(atom)$			Formation energies (eV) for two excess Mo atoms (Fig. 5 (b)) $\mu_{Mo}=\mu_{Mo}(dimer)$		
		Adatom	Split int.	Interst.	Addimer	Split-pair	Int-pair
MoS_2	3.18	-1.48	**-2.51**	0.14	**-0.74**	0.91	1.45
$MoSe_2$	3.32	-1.05	**-2.26**	-1.72	-0.46	1.13	**-1.35**
$MoTe_2$	3.55	-1.08	-2.15	**-3.85**	-0.60	0.01	**-4.48**

Table 1. Formation energies for all configurations shown in Fig. 4. Calculated lattice constants are also shown. Bold text highlights the most stable configuration. For defects with single Mo atom, we choose a reference corresponding to Mo atom in vacuum. For defects with two Mo atoms, we choose a reference with a Mo dimer in vacuum.

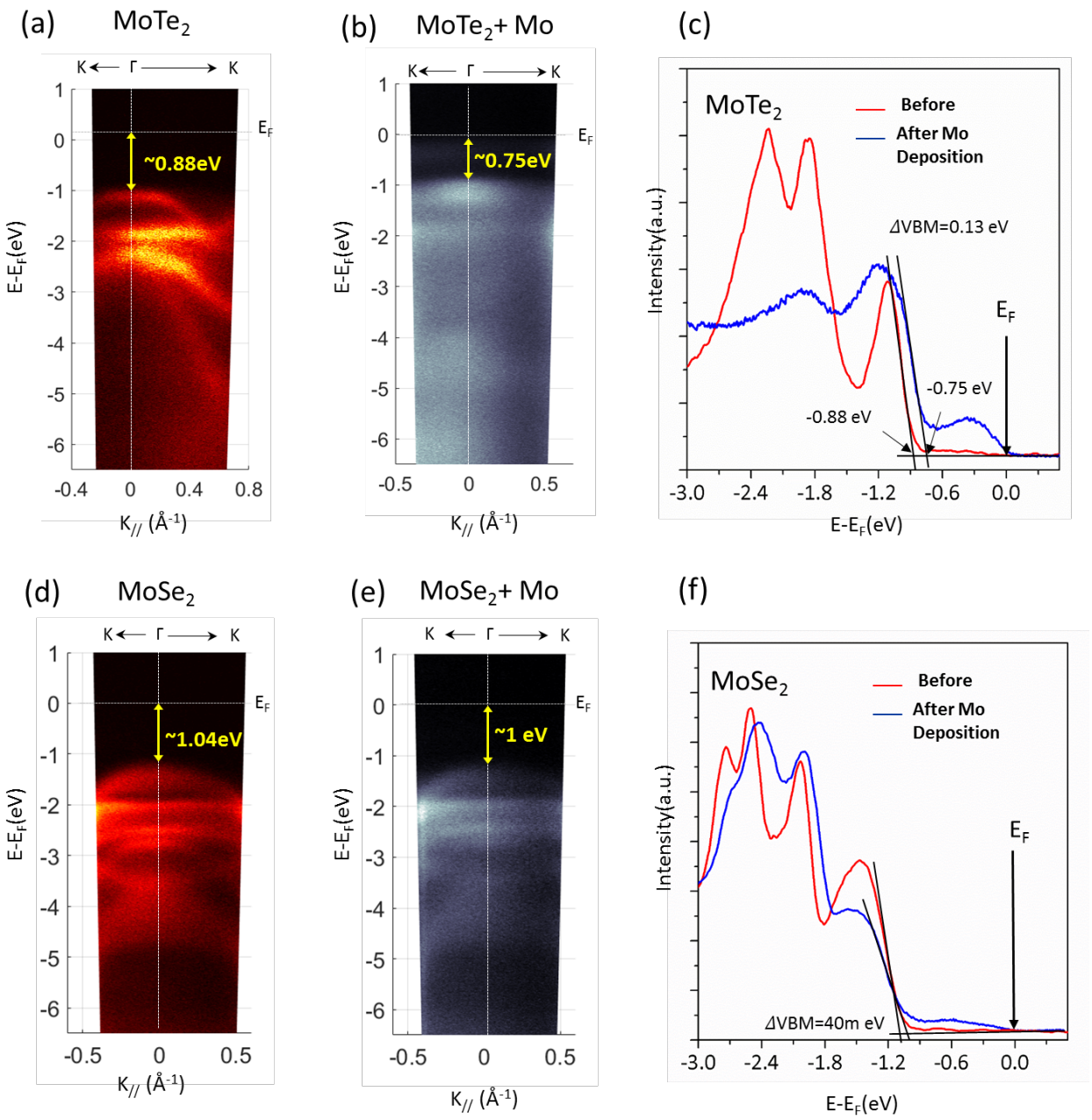

Figure 7. ARPES studies of $MoTe_2$ and $MoSe_2$ single crystal surface before and after MTB formation in the vicinity of the Γ-point. He-II ARPES spectra of the $MoTe_2$ single crystal before and after Mo deposition at 350˚C are shown in (a) and (b), respectively. The comparison of energy distribution curves of the electron densities at the Γ-point, before and after Mo deposition, is shown in (c). He-II ARPES spectra of the $MoSe_2$ single crystal before and after Mo deposition at 350˚C are shown in (d) and (e), respectively. The comparison of energy distribution curves of the electron densities at the Γ-point, before and after Mo deposition, is shown in (f). The lower concentration of MTBs in $MoSe_2$ compared to $MoTe_2$ gives rise to the weaker intensity close to the Fermi-level for the $MoSe_2$ sample

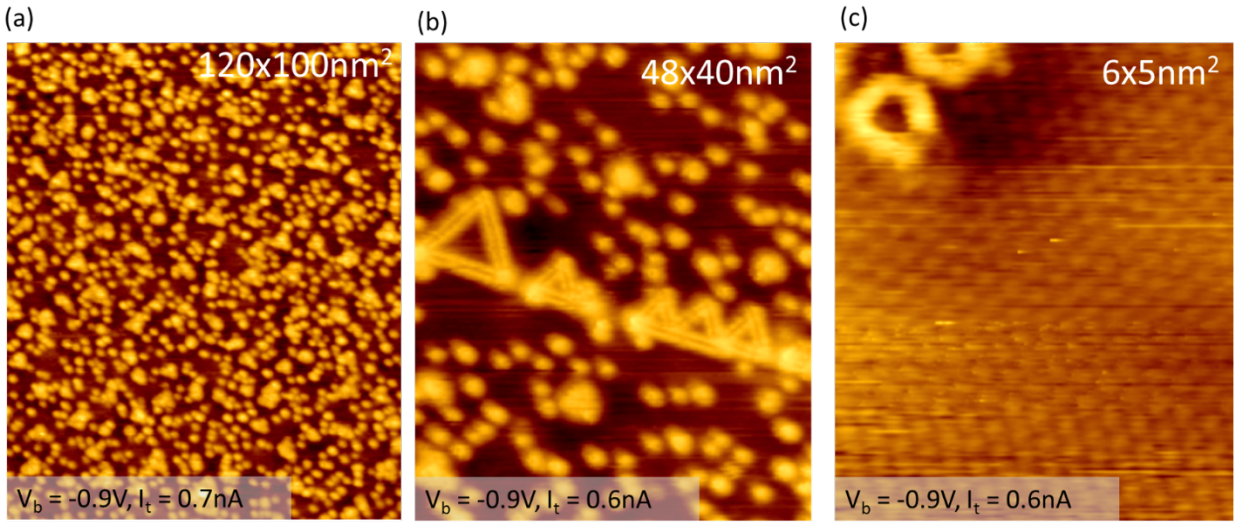

Figure 8: STM of 0.3% of a titanium ML deposited on $MoTe_2$ at 350 ˚C (a) Large scale image showing single protrusions together with some small triangular MTBs. (b) some larger triangular MTB-loops are occasionally observed that appear to be aligned and thus suggesting that some pre-existing line defect in the substrate may assist their formation. (c) Zoom-in on bright protrusions shows a similar ring structure as has been observed for single Mo-interstitial sites, suggesting that every protrusion is due to a Ti-interstitial.

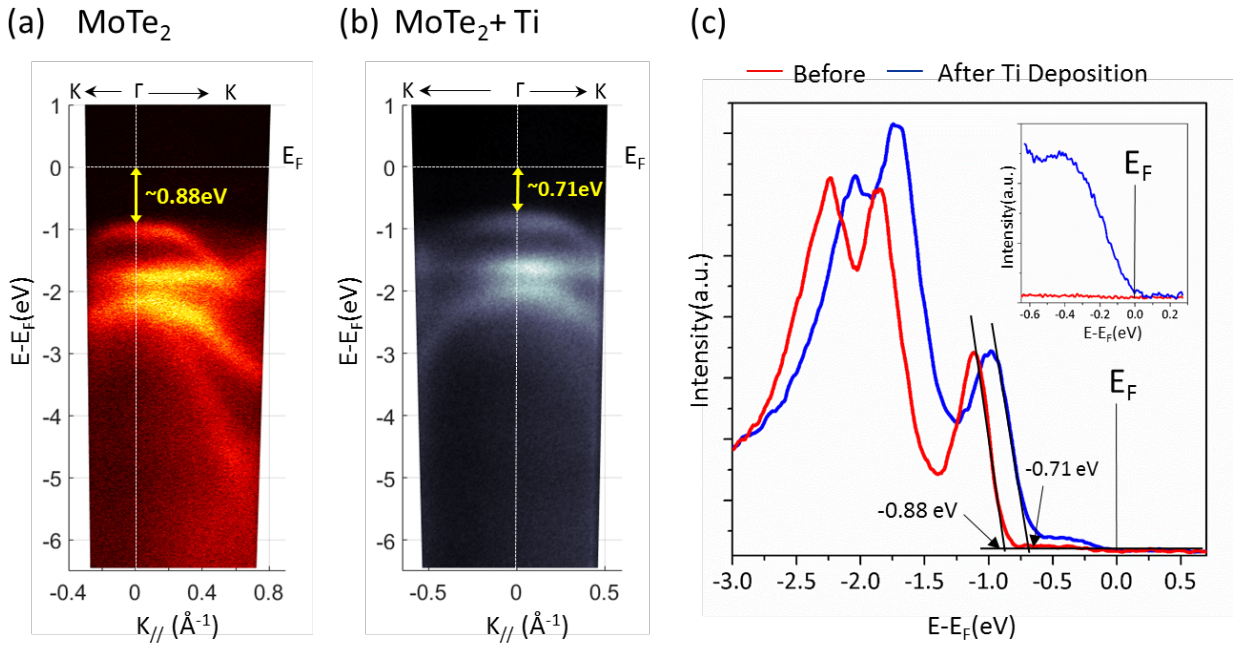

Figure 9: ARPES studies of MoTe2 and $MoTe_2$+Ti. . He-II ARPES spectra of the $MoTe_2$ single crystal before and after Ti deposition at 350˚C are shown in (a) and (b) respectively. (c) Comparison of energy distribution curves at the Γ-point, before and after Ti deposition. The inset shows the electron densities close to the fermi-level.

References:

[1] Wei, X.; Wang, M.-S.; Bando, Y.; Golberg, D. Electron-Beam-Induced Substitutional Carbon Doping of Boron Nitride Nanosheets, Nanoribbons, and Nanotubes. *ACS Nano* **2011**, *5*, 2916–2922.

[2] Wang, H.; Wang, Q.; Cheng, Y.; Li, K.; Yao, Y.; Zhang, Q.; Dong, C.; Wang, P.; Schwingenschlögl, U.; Yang, W.; Zhang, X.X. Doping Monolayer Graphene with Single Atom Substitutions. *Nano Lett.* **2012***, 12*, 141–144.

[3] Lin, Y.-C.; Björkman, T.; Komsa, H.-P.; Teng, P.-Y.; Yeh, C.-H.; Huang, F.-S.; Lin, K.-H.; Jadczak, J.; Huang Y.-S.; Chiu, P.W.; Krasheninnikov, A.V.; Suenaga, K. Three-fold rotational defects in two-dimensional transition metal dichalcogenides. *Nat. Commun.* **2015**, *6*, 6736.

[4] Sutter, E.; Huang, Y.; Komsa, H.-P.; Ghorbani-Asl, M., Krasheninnikov, A.V., Sutter, P. Electron-Beam Induced Transformations of Layered Tin Dichalcogenides. *Nano Lett.* **2016***, 16*, 4410-4416.

[5] Lin, Y.-C.; Dumcenco, D.O.; Huang, Y-S.; Suenaga, K. Atomic mechanism of the semiconducting-to-metallic phase transition in single-layered MoS_2. *Nat. Nano.* **2014**, *9,* 391–396.

[6] Kappera, R.; Voiry, D.; Yalcin, S.E.; Branch, B.; Gupta, G.; Mohite, A.D.; Chhowalla, M. Phase-engineered low-resistance contacts for ultrathin MoS_2 transistors. *Nat. Mater.* **2014**, *13,* 1128–1134.

[7] Wang, Y.; Xiao, J.; Zhu, H.; Li, Y.; Alsaid, Y.; Fong, K.Y.; Zhou, Y.; Wang, S.; Shi, W.; Wang, Y.; Zettl, A.; Reed, E.J.; Zhang, X. Structural phase transition in monolayer $MoTe_2$ driven by electrostatic doping. *Nature* **2017**, *550*, 487-491.

[8] Ma, Q.; Isarraraz, M.; Wang, C.S.; Preciado, E.; Klee, V.; Bobek, S.; Yamaguchi, K.; Li, E.; Odenthal, P.M.; Nguyen, A.; Barroso, D.; Sun, D.; von Son Palacio, G.; Gomez, M.; Nguyen, A.; Le, D.; Pawin, G.; Mann, J.; Heinz, T.F.; Rahman, T.S.; Bartels, L. Postgrowth Tuning of the Bandgap of Single-Layer Molybdenum Disulfide Films by Sulfur/Selenium Exchange. *ACS Nano* **2014**, *8*, 4672–4677.

[9] Huang, C.; Wu,S.; Sanchez, A.M.; Peters, J.J.P.; Beanland, R.; Ross, J.S.; Rivera, P.; Yao, W.; Cobden, D.H.; Xu , X. Lateral heterojunctions within monolayer $MoSe_2$–WSe_2 semiconductors. *Nat. Mater.* **2014**, *13*, 1096–1101.

[10] Sutter, P.; Huang, Y.; Sutter, E. Nanoscale Integration of Two-Dimensional Materials by Lateral Heteroepitaxy. *Nano Lett.* **2014***, 14,* 4846–4851.

[11] Lehtinen, O.; Komsa, H.-P.; Pulkin, A.; Whitwick, M.B.; Chen, M.W., Lehnert, T.; Mohn, M.J.; Yazyev, O.V.; Kis, A.; Kaiser, U.; Krasheninnikov, A.V. Atomic Scale Microstructure and Properties of Se-Deficient Two-Dimensional $MoSe_2$. *ACS Nano* **2015**, *9*, 3274–3283.

[12] Lin, J.; Pantelides, S.T.; Zhou, W. Vacancy-Induced Formation and Growth of Inversion Domains in Transition-Metal Dichalcogenide Monolayer. *ACS Nano* **2015**, *9*, 5189–5197.

[13] van der Zande, A.M.; Huang, P.H.; Chenet, D.A.; Berkelbach, T.C.; You, Y.M.; Lee, G.-H.; Heinz, T.F.; Reichman, D.R.; Muller, D.A.; Hone, J.C. Grains and grain boundaries in highly crystalline monolayer molybdenum disulphide. *Nat. Mater.* **2013**, *15*, 554–561.

[14] Ly, T.H.; Perello, D.J.; Zhao, J.; Deng, Q.; Kim, H.; Han G.H.; Chae, S.H.; Jeong, H.Y.; Lee, Y.H. Misorientation-angle-dependent electrical transport across molybdenum disulfide grain boundaries. *Nat. Commun.* **2016**, *7*, 10426.

[15] Zhang, Z.; Zou, X.; Crespi, V.H.; Yakobson, B.I. Intrinsic Magnetism of Grain Boundaries in Two-Dimensional Metal Dichalcogenides. *ACS Nano* **2013**, *7*, 10475–10481.

[16] Ma, Y.; Kolekar, S.; Coy Diaz, H.; Aprojanz, J.; Miccoli, I.; Tegenkamp, C.; Batzill, M. Metallic Twin Grain Boundaries Embedded in $MoSe_2$ Monolayers Grown by Molecular Beam Epitaxy. *ACS Nano* **2017**, *11*, 5130-5139.

[17] Zhou, W.; Zou, X.; Najmaei, S.; Liu, Z.; Shi, Y.; Kong, J.; Lou, J.; Ajayan, P. M.; Yakobson, B. I.; Idrobo, J. C.Intrinsic Structural Defects in Monolayer Molybdenum Disulfide *Nano Lett.* **2013**, *13*, 2615–2622.

[18] Komsa, H.-P.; Krasheninnikov, A.V. Engineering the Electronic Properties of Two-Dimensional Transition Metal Dichalcogenides by Introducing Mirror Twin Boundaries. *Adv. Electr. Mater.* **2017**, *3*, 1600468.

[19] Liu, L.; Jiao, L.; Yang, F.; Cai, Y.; Wu, X.; Ho, W.; Gao, C.; Jia, J.; Wang, N.; Fan, H.; Yao, W.; Xie, M. Dense Network of One-Dimensional Midgap Metallic Modes in Monolayer $MoSe_2$ and Their Spatial Undulations. *Phys. Rev. Lett.* **2014**, *113*, 066105.

[20] Coy Diaz, H.; Ma, Y.; Chaghi, R.; Batzill, M. High Density of (Pseudo) Periodic Twin-Grain Boundaries in Molecular Beam Epitaxy-Grown van der Waals Heterostructure: $MoTe_2/MoS_2$. *Appl. Phys. Lett.* **2016**, *108*, 191606

[21] Zou, X.; Liu, Y.; Yakobsen, B. I. Predicting Dislocations and Grain Boundaries in Two-Dimensional Metal-Disulfides from First Principles. *Nano Lett.* **2013**, *13*, 253–258.

[22] Ma, Y.; Coy Diaz, H.; Avila, J.; Chen, C.; Kalappattil, V.; Das, R.; Phan, M.-H.; Cadez, T.; Carmelo, J. M. P.; Asensio, M. C.; Batzill, M. Angle Resolved Photoemission Spectroscopy Reveals Spin Charge Separation in Metallic $MoSe_2$ Grain Boundary. *Nat. Commun.* **2017**, *8*, 14231.

[23] Barja, S.; Wickenburg, S.; Liu, Z.-F.; Zhang, Y.; Ryu, H.; Ugeda, M. M.; Hussain, Z.; Shen, Z.-X.; Mo, S.-K.; Wong, E.; Salmeron, M. B.; Wang, F.; Crommie, M. F.; Ogletree, D. F.; Neaton, J. B.; Weber-Bargioni, A. Charge Density Wave Order in 1D Mirror Twin Boundaries of Single-Layer $MoSe_2$. *Nat. Phys.* **2016**, *12*, 751.

[24] Herbig, C.; Knispel, T.; Simon, S.; Schröder, U.A; Martínez-Galera, A.J.; Arman, M.A.; Teichert, C.; Knudsen, J.; Krasheninnikov, A.V.; Michely, T. From Permeation to Cluster Arrays: Graphene on Ir(111) Exposed to Carbon Vapor. *Nano Lett.* **2017**, *17*, 3105–3112.

[25] Chou, S.S; Sai, N.; Lu, P.; Coker, E.N.; Liu, S.; Artyushkova, K.; Luk, T.S.; Kaehr, B.; Brinker, C.J. Understanding catalysis in a multiphasic two-dimensional transition metal dichalcogenide. *Nat. Commun.* **2015**, *6* ,8311.

[26] Seok, J.;Lee, J.-H.; Cho, S.; Ji, B.; Kim, H.W.; Kwon, M.; Kim, D.; Kim, Y.-M.; Oh, S.H.; Kim, S.W.; Lee, Y.H.; Son, Y.-W.; Yang, H. Active hydrogen evolution through lattice distortion in metallic $MoTe_2$. *2D Mater.* **2017**, *4*, 025061.

[27]Sung, J.H.; Heo, H.; Si, S.; Kim, Y.H.; Noh, H.R.; Song, K.; Kim, J.; Lee, C.-S.; Seo, S.-Y.; Kim, D.-H.; Kim, H.K.; Yeom, H.W.; Kim, T-H.; Choi, S.-Y.; Kim, J.S.; Jo, M.-H. Coplanar semiconductor–metal circuitry defined on few-layer MoTe2 via polymorphic heteroepitaxy. *Nat. Nano.* **2017**, *12*, 1064-1070.

[28] Cho, S.; Kim, S.; Kim, J.H.; Zhao, J.; Seok, J.; Keum, D.H.; Baik, J.; Choe, D.-H.; Chang, J.J.; Suenaga,K.; Kim, S.W.; Lee, Y.H.; Yang, H. Phase patterning for ohmic homojunction contact in $MoTe_2$. *Science* **2015**, 625-628.

[29] Qi, D.; Wang, Q.; Han, C.; Jiang, J.; Zheng, Y.; Chen, W.; Zhang, W.; Wee, A.T.S. Reducing the Schottky barrier between few-layer $MoTe_2$ and gold. *2D Mater.* **2017**, *4*, 045016.

[30] Diaz, H.C.; Chaghi, R.; Ma, Y.; Batzill, M. Molecular beam epitaxy of the van der Waals heterostructure $MoTe_2$ on MoS_2: phase, thermal, and chemical stability. *2D Materials* **2015**, *2*, 044010.

[31]Addou, R.; McDonnell, S.; Barrera, D; Guo, Z.B.; Azcatl, A.; Wang, J.; Zhu, H.; Hinkle, C.L.; Quevedo-Lopez, M.; Alshareef, H.N.; Colombo, L.; Hsu, J.W.P.; Wallace, R.M. Impurities and Electronic Property Variations of Natural MoS_2 Crystal Surfaces. *ACS Nano* **2015**, *9*, 9124-9133.

[32] Hong, J.; Wang, C.; Liu, H.; Ren, X.; Chen, J.; Wang, G.; Jia, J.; Xie, M.; Jin, C.; Ji, W.; Yuan, J.; Zhang, Z. Inversion Domain Boundary Induced Stacking and Bandstructure Diversity in Bilayer $MoSe_2$. *Nano Lett.* **2017**, *17*, 6653–6660.

[33] Allain, A.; Kang, J.; Banerjee, K.; Kis, A. Electrical contacts to two-dimensional semiconductors. *Nat. Mater.* **2015**, *14*, 1195-1205.

[34] Kresse, G.; Hafner, J. *Ab. initio* molecular dynamics for liquid metals *Phys. Rev. B* **1993**, *47*, 558 - 561; *Ab initio* molecular-dynamics simulation of the liquid-metal–amorphous-semiconductor transition in germanium. *Phys. Rev. B* **1994**, *49*, 14251- 14269.

[35] Henkelman, G; Uberuaga, B.P.; Jónsson, H. A climbing image nudged elastic band method for finding saddle points and minimum energy paths. *J. Chem. Phys.* **2000**, *113*, 9901-9904.